Journal of Alloys and Compounds 480 (2009) 547–553

Contents lists available at ScienceDirect

Journal of Alloys and Compounds

journal homepage: www.elsevier.com/locate/jallcom

# Investigation on the structures and electrochemical performances of $La_{0.75-x}Zr_xMg_{0.25}Ni_{3.2}Co_{0.2}Al_{0.1}$ ($x = 0$–$0.2$) electrode alloys prepared by melt spinning

Yang-huan Zhang[a,b,*], Bao-wei Li[b], Hui-ping Ren[b], Shi-hai Guo[a], Qi Yan[a], Xin-lin Wang[a]

[a] Department of Functional Material Research, Central Iron and Steel Research Institute, Beijing 100081, China
[b] School of Material, Inner Mongolia University of Science and Technology, Baotou 014010, China

ARTICLE INFO

*Article history:*
Received 5 December 2008
Received in revised form 17 January 2009
Accepted 24 January 2009
Available online 6 February 2009

*Keywords:*
$A_2B_7$-type electrode alloy
Substitution of Zr for La
Melt-spinning
Microstructure
Electrochemical performance

ABSTRACT

In order to improve the electrochemical cycle stability of the La–Mg–Ni system $A_2B_7$-type electrode alloys, La in the alloy was partially substituted by Zr and the melt-spinning technology was used for preparing $La_{0.75-x}Zr_xMg_{0.25}Ni_{3.2}Co_{0.2}Al_{0.1}$ ($x = 0$, 0.05, 0.1, 0.15, 0.2) electrode alloys. The microstructures and electrochemical performances of the as-cast and quenched alloys were investigated in detail. The results obtained by XRD, SEM and TEM showed that the as-cast and quenched alloys have a multiphase structure which is composed of two main phases (La, Mg)$Ni_3$ and $LaNi_5$ as well as a residual phase $LaNi_2$. The substitution of Zr for La leads to an obvious increase of the $LaNi_5$ phase in the alloys, and it also helps the formation of a like amorphous structure in the as-quenched alloy. The results of the electrochemical measurement indicated that the substitution of Zr for La obviously decreased the discharge capacity of the as-cast and quenched alloys, but it significantly improved their cycle stability. The discharge capacity of the alloys ($x \leq 0.1$) first increased and then decreased with the variety of the quenching rate. The cycle stability of the alloys monotonously rose with increasing quenching rate.



## 1. Introduction

Considerable attention has been paid to for the development of high performance hydrogen storage alloys used as the negative electrode of Ni–MH batteries. Consequently, a series of metal hydride electrode materials have been discovered, such as the rare-earth-based $AB_5$-type alloys [1], the $AB_2$-type Laves phase alloys [2], the V-based solid solution alloys [3], and the Mg-based alloys [4]. The production of $AB_5$-type hydrogen storage alloy has been commercialised in many countries, especially in USA, Japan and China [5,6].

Recently, Europe community and major developed countries in the world issued in succession a decree forbidding the Ni–Cd battery to be continually used, which provides a golden opportunity for the development of the Ni–MH battery. However, none of the above-mentioned candidate alloys can meet the demand of the power battery owing to the limitation of their properties. Therefore, it has been one of the main challenges faced by researchers in this area to find new type electrode alloys with higher capacity and longer cycle life. Recently, some of the new series of R–Mg–Ni-based (where R is a rare earth or Y, Ca) $A_2B_7$-type alloys were considered to be most promising candidates owing to their higher discharge capacities (360–410 mAh/g) and low production costs. Kohno et al. [7] found that the $La_5Mg_2Ni_{23}$-type electrode alloy $La_{0.7}Mg_{0.3}Ni_{2.8}Co_{0.5}$ has a capacity of 410 mAh/g, and good cycle stability during 30 charge–discharge cycles. Liu et al. [8] revealed that the $La_{0.7}Mg_{0.3}(Ni_{0.85}Co_{0.15})_{3.5}$ alloy had a multi-phases structure, and two major phases were found, e.g. a (La, Mg)$Ni_3$ phase with the $PuNi_3$-type rhombohedral structure in space group $R\bar{3}m$ and a $LaNi_5$ phase with the $CaCu_5$-type hexagonal structure in space group $P6/mmm$. Pan et al. [9] investigated the structures and electrochemical characteristics of the $La_{0.7}Mg_{0.3}(Ni_{0.85}Co_{0.15})_x$ ($x = 3.15$–$3.80$) alloy system and obtained a maximum discharge capacity of 398.4 mAh/g, but the cycle stability of the alloy needs to be improved further. Pan et al. [10] and Liao et al. [11] researched the influence of element additives and substitution on the structure and electrochemical behaviours of the alloys, and the results showed that the addition and substitution of elements Al, Cu, Fe, Mn, Co and Zr significantly improved the electrochemical performances of the alloys.

Although the investigation on the structure and electrochemical properties of the alloys has obtained very important progress, their poor cycle stability has to be further improved for commercial application. It is well known that element substitution is one

* Corresponding author at: Department of Functional Material Research, Central Iron and Steel Research Institute, 76 Xueyuan Nan Road, Haidian District, 100081 Beijing, China. Tel.: +86 10 62187570; fax: +86 10 62182296.
*E-mail address:* zyh59@yahoo.com.cn (Y.-h. Zhang).

0925-8388/$ – see front matter © 2009 Elsevier B.V. All rights reserved.
doi:10.1016/j.jallcom.2009.01.090

of the effective methods for improving the overall properties of the hydrogen storage alloys. In addition, the preparation technology is also extremely important for improving the performances of the alloys. Especially, our previous works confirmed that melt-spinning treatment can significantly improve the cycle stability of the La–Mg–Ni system $A_2B_7$-type alloys [12,13]. Therefore, it is expected that the combination of an optimized amount of Zr substitution with a proper rapid quenching technique may lead to an alloy with high discharge capacity and good cycling stability. For this purpose, the effects of substituting La with Zr and rapid quenching technique on the microstructures and electrochemical characteristics of $La_{0.75-x}Zr_xMg_{0.25}Ni_{3.2}Co_{0.2}Al_{0.1}$ ($x$ = 0–0.2) alloys were systematically investigated.

## 2. Experimental

The nominal compositions of the experimental alloys were $La_{0.75-x}Zr_xMg_{0.25}Ni_{3.2}Co_{0.2}Al_{0.1}$ ($x$ = 0, 0.05, 0.1, 0.15, 0.2). For convenience, the alloys were denoted with Zr content as $Zr_0$, $Zr_1$, $Zr_2$, $Zr_3$ and $Zr_4$, respectively. The alloy ingots were prepared using a vacuum induction furnace in a helium atmosphere at a pressure of 0.04 MPa. Part of the as-cast alloys was re-melted and quenched by melt-spinning with a rotating copper roller. The quenching rate was approximately expressed by the linear velocity of the copper roller because it is too difficult to measure a real quenching rate, i.e. cooling rate of the sample during quenching. The quenching rates used in the experiment were 5, 10, 15 and 20 m/s, respectively.

The cast ingot and quenched ribbons were mechanically crushed and ground into the powder of 300 mesh size for X-ray diffraction (XRD). The phase structures and compositions of the alloys were determined by XRD diffractometer of D/max/2400. The diffraction, with the experimental parameters of 160 mA, 40 kV and 10°/min respectively, was performed with $CuK_{\alpha 1}$ radiation filtered by graphite. The morphologies of the as-cast and quenched alloys were examined by SEM. The powder samples of the as-quenched alloys were dispersed in anhydrous alcohol for observing the grain morphology with TEM, and for determining crystalline state of the samples with selected area electron diffraction (SAD).

Round electrode pellets of 15 mm in diameter were prepared by cold pressing a mixture of alloy powder and carbonyl nickel powder in the weight ratio of 1:4 with a pressure of 35 MPa. After dried for 4 h, the electrode pellets were immersed in a 6 M KOH solution for 24 h in order to wet fully the electrodes before the electrochemical measurement.

A tri-electrode open cell, consisting of a metal hydride electrode, a $NiOOH/Ni(OH)_2$ counter electrode and a Hg/HgO reference electrode, was used for testing the electrochemical performance of the experimental electrodes. The electrolyte was a 6 M KOH solution. The voltage between the negative electrode and the reference electrode was defined as the discharge voltage. In every cycle, the alloy electrode was firstly charged with a constant current density. After resting 15 min, it was discharged at a same current density to cut-off voltage of −0.500 V. The environment temperature of the measurement was kept at 30 °C.

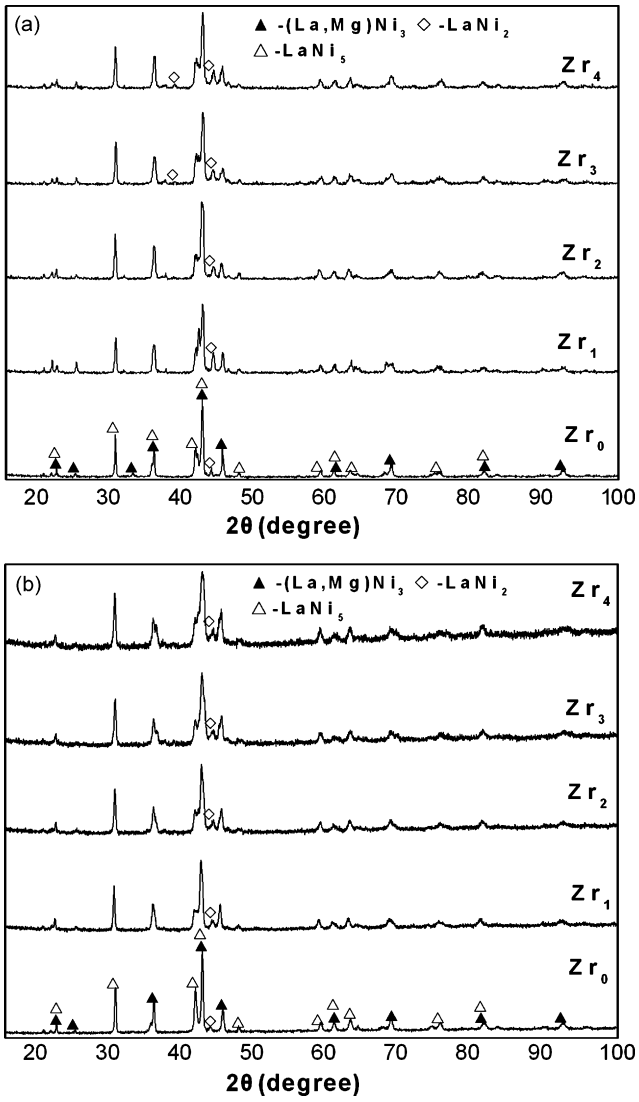


**Fig. 1.** XRD patterns of the as-cast and quenched (20 m/s) alloys: (a) as-cast, (b) as-quenched.

**Table 1**
Lattice constants and abundances of $LaNi_5$ and (La, Mg)$Ni_3$ major phases.

| Conditions | Alloys | Major phases | Lattice constants (nm) | | Cell volume (nm$^3$) | Phase abundance (wt.%) |
|---|---|---|---|---|---|---|
| | | | $a$ | $c$ | | |
| As-cast | $Zr_0$ | (La, Mg)$Ni_3$ | 0.5204 | 2.4401 | 0.5722 | 74.35 |
| | | $LaNi_5$ | 0.5197 | 0.4178 | 0.0977 | 24.07 |
| | $Zr_1$ | (La, Mg)$Ni_3$ | 0.5147 | 2.4359 | 0.5596 | 67.67 |
| | | $LaNi_5$ | 0.5132 | 0.4104 | 0.0936 | 30.62 |
| | $Zr_2$ | (La, Mg)$Ni_3$ | 0.5082 | 2.4301 | 0.5435 | 64.89 |
| | | $LaNi_5$ | 0.5063 | 0.4079 | 0.0905 | 33.05 |
| | $Zr_3$ | (La, Mg)$Ni_3$ | 0.5034 | 2.4251 | 0.5322 | 61.55 |
| | | $LaNi_5$ | 0.5012 | 0.4052 | 0.0881 | 36.21 |
| | $Zr_4$ | (La, Mg)$Ni_3$ | 0.4966 | 2.4167 | 0.5161 | 58.33 |
| | | $LaNi_5$ | 0.4936 | 0.4018 | 0.0848 | 39.24 |
| As-quenched (20 m/s) | $Zr_0$ | (La, Mg)$Ni_3$ | 0.5197 | 2.4409 | 0.5709 | 71.52 |
| | | $LaNi_5$ | 0.5189 | 0.4183 | 0.0975 | 26.27 |
| | $Zr_1$ | (La, Mg)$Ni_3$ | 0.5139 | 2.4366 | 0.5411 | 65.83 |
| | | $LaNi_5$ | 0.5129 | 0.4109 | 0.0936 | 31.84 |
| | $Zr_2$ | (La, Mg)$Ni_3$ | 0.5067 | 2.4318 | 0.5406 | 63.04 |
| | | $LaNi_5$ | 0.5052 | 0.4093 | 0.0905 | 34.22 |
| | $Zr_3$ | (La, Mg)$Ni_3$ | 0.5029 | 2.4251 | 0.5311 | 60.32 |
| | | $LaNi_5$ | 0.5009 | 0.4053 | 0.0881 | 36.66 |
| | $Zr_4$ | (La, Mg)$Ni_3$ | 0.4961 | 2.4180 | 0.5153 | 57.27 |
| | | $LaNi_5$ | 0.4932 | 0.4022 | 0.0847 | 39.49 |

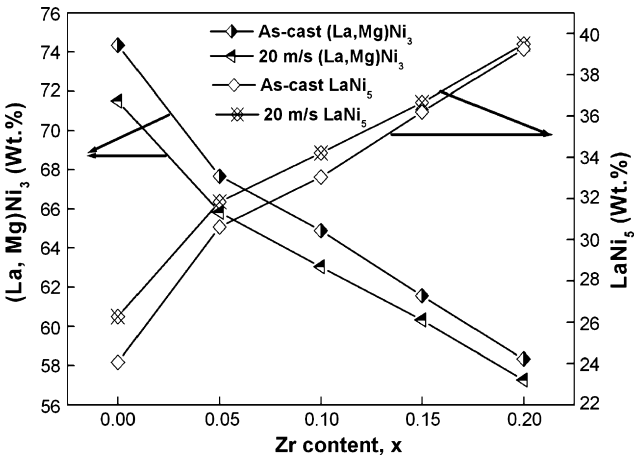


**Fig. 2.** Evolution of the abundances of the major phases $LaNi_5$ and (La, Mg)$Ni_3$ with Zr content.

## 3. Results

### 3.1. Structural characteristics

Shown in Fig. 1 is the XRD patterns of the cast and quenched (20 m/s) alloys, revealing that the as-cast and quenched alloys hold a multiphase structure, composing of two major phases (La, Mg)$Ni_3$ and $LaNi_5$ as well as a residual phase $LaNi_2$. The substitution of Zr for La exerted an unconscious influence on the phase compositions of the alloys, and the major diffraction peaks of the $LaNi_5$ and the (La, Mg)$Ni_3$ phases in the alloys obviously tend to overlap with the increase of Zr content. Listed in Table 1 were the lattice parameters of $LaNi_5$ and (La, Mg)$Ni_3$ major phases in the as-cast and quenched (20 m/s) alloys, which were calculated from the XRD data by a software of Jade 6.0. The results showed that the substitution of Zr for La obviously reduced the lattice constants and cell volumes of $LaNi_5$ and (La, Mg)$Ni_3$ major phases in the alloys, which is due to the fact that the atom radius of Zr is smaller than that of La. It is derived by Table 1 that the substitution of Zr for La caused an increase of the $LaNi_5$ phase and a decrease of the (La, Mg)$Ni_3$ phase. In order to distinctly show the influence of Zr content on the abundances of the major phases in the alloys, the Zr content dependence of the abundances of the $LaNi_5$ and the (La, Mg)$Ni_3$ major phases in the as-cast and quenched (20 m/s) alloys was plotted in Fig. 2. It can clearly be seen in Fig. 2 that the rapid quenching leads to an increase of the $LaNi_5$ phase and a decrease of the (La, Mg)$Ni_3$ phase.

The images of the as-cast alloys taken by SEM were shown in Fig. 3. The result obtained by SEM with an energy dispersive spectrometry (EDS) indicated that all the experimental alloys are of multiphase structure, containing both (La, Mg)$Ni_3$ and $LaNi_5$ phases, which is in agreement with the results by XRD. Because the amount of the $LaNi_2$ phase is small and it attaches itself to the (La, Mg)$Ni_3$ phase in the process of growing, so, it is difficult to observe the morphology of the $LaNi_2$ phase. It can be seen in Fig. 3 that the substitution of Zr for La leads to the grains of the as-cast alloys significantly refined.

The morphologies and the crystalline states of the as-quenched alloys were examined by TEM as shown in Fig. 4. The figure indicated that as-quenched (20 m/s) $Zr_0$ alloy exhibits a nanocrystalline and microcrystalline structure. The electron diffraction pattern of $Zr_4$ alloy show broad and dull halo, meaning a like amorphous structure formed. In order to confirm the diffuse pattern is not from an over-exposure of the electron diffraction, several exposures were made of differing intensity/time and they all showed very similar diffuse pattern for the $Zr_4$ alloy. This seems to be conflicting with the result in Fig. 1 due to without an amorphous phase found by XRD. A probable reason is that the like amorphous phase forms at some selective location in the as-quenched alloy and its amount is very small, so, the XRD patterns did not clearly exhibit the presence of an amorphous phase. Based on the result in Fig. 4, it can be concluded that the substitution of Zr for La favors the formation of an amorphous phase in the as-quenched alloy.

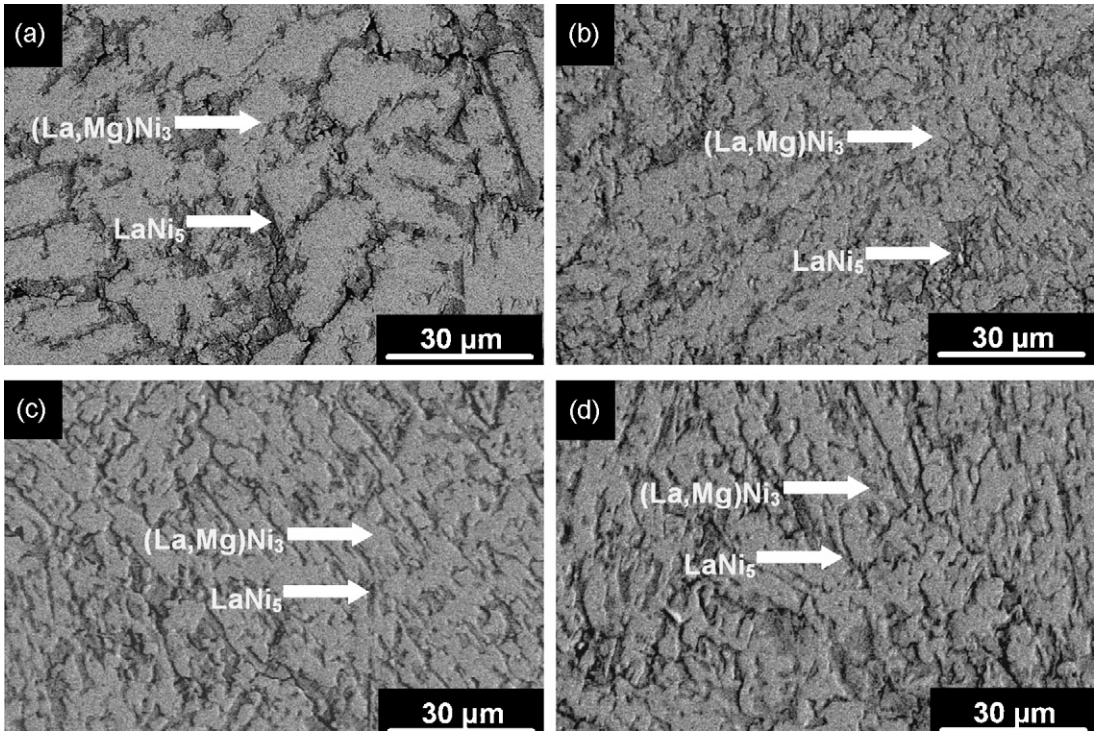


**Fig. 3.** Images of the as-cast alloys taken by SEM: (a) $Zr_0$, (b) $Zr_1$, (c)$Zr_2$, (d) $Zr_4$.

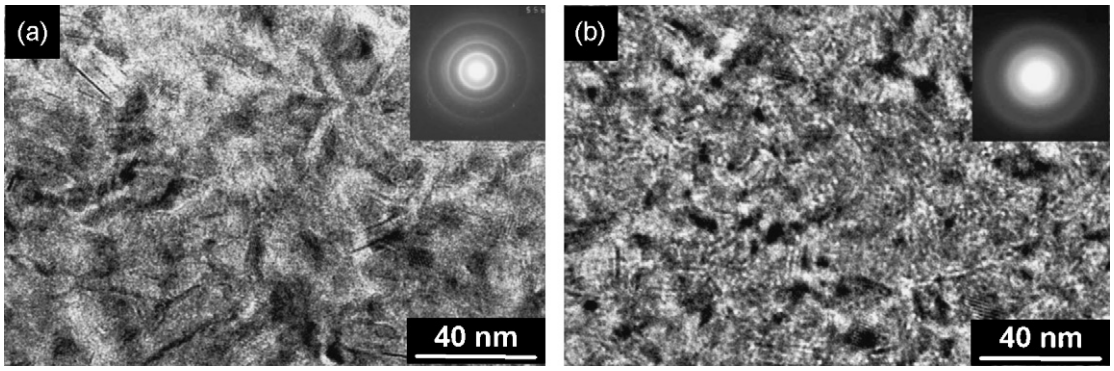


**Fig. 4.** Morphologies and SAD of the as-quenched alloys (20 m/s) taken by TEM: (a) $Zr_0$, (b) $Zr_4$.

### 3.2. Electrochemical performances

#### 3.2.1. Activation capability and discharge capacity

The activation capability was characterized by the number of charging–discharging cycles required for attaining the greatest discharge capacity through a charging–discharging cycle at a constant current density of 100 mA/g. The fewer the number of charging–discharging cycle, the better the activation performance. The evolution of the discharge capacities of the as-cast and quenched alloys with the cycle number was plotted in Fig. 5, indicating that all the as-cast and quenched alloys display excellent activation performances, attaining their maximum discharge capacities after 1–2 charging–discharging cycles. The substitution of Zr for La slightly impairs the activation capability of the as-cast alloys.

The quenching rate dependence of the maximum discharge capacities of the alloys was shown in Fig. 6, for a charge–discharge current density of 100 mA/g. It can be derived from Fig. 6 that for a fixed quenching rate the discharge capacity of the alloy decreases with increasing Zr content. When Zr content increases from 0 to 0.2, the discharge capacity of the as-cast alloy declines from 389.4 to 357.2 mAh/g, and from 374 to 337.4 mAh/g for the quenching rate of 20 m/s, respectively. It can clearly be seen in Fig. 6 that with the incremental change of the quenching rate the discharge capacities of the alloys ($x \leq 0.10$) first increase and then decrease, but the discharge capacities of the alloys ($x > 0.10$) monotonously falls. When the quenching rate rises from 0 to 20 m/s, the discharge capacity increases from 371.6 (0 m/s) to 374.7 (5 m/s), after that drops to 357.6 mAh/g (20 m/s) for the $Zr_2$ alloy, and it monotonously declines from 357.2 to 337.4 mAh/g for the $Zr_4$ alloys.

#### 3.2.2. High rate discharge ability (HRD)

The high rate discharge (HRD) ability of the alloy electrode, which was mainly determined by the kinetic property, was calculated according to following formula: HRD = $C_{600,max}/C_{100,max} \times 100\%$, where $C_{600,max}$ and $C_{100,max}$ are the maximum discharge capacities of the electrode charged–discharged at the current densities of 600 and 100 mA/g respectively. The HRDs of the alloys as a function of the quenching rate were shown in Fig. 7. It can be seen that the HRDs of the $Zr_0$, $Zr_1$ and $Zr_2$ alloys obtain the maximum value with the variety of the quenching rate. But the HRDs of the $Zr_3$ and $Zr_4$ alloys monotonously decrease with increasing quenching rate. When the quenching rate increases from 0 to 20 m/s, the HRD of the $Zr_1$ alloy increases from 89.22% to 91.02% and then decreases to 80.12%, whereas that of the $Zr_4$ alloy monotonously falls from 77.65% to 65.66%.

#### 3.2.3. Cycle stability

The capacity retaining rate ($S_{100}$) is introduced for accurately evaluating the cycle stability of the alloy. It is defined as $S_n = C_n/C_{max} \times 100\%$, where $C_{max}$ is the maximum discharge capacity, and $C_n$ is the discharge capacity of the $n$th cycle at a current density of 600 mA/g, respectively. The capacity retaining rate ($S_{100}$) of the as-cast and quenched alloys as a function of Zr content was illustrated in Fig. 8, indicating that the substitution of Zr for La leads to the capacity retaining rates ($S_{100}$) of the alloys significantly increased. When Zr content rises from 0 to 0.2, the capacity retaining rate ($S_{100}$) increases from 65.32% to 76.69% for the as-cast alloy, and from 73.97% to 85.18% for as-quenched (20 m/s) alloy. It can also

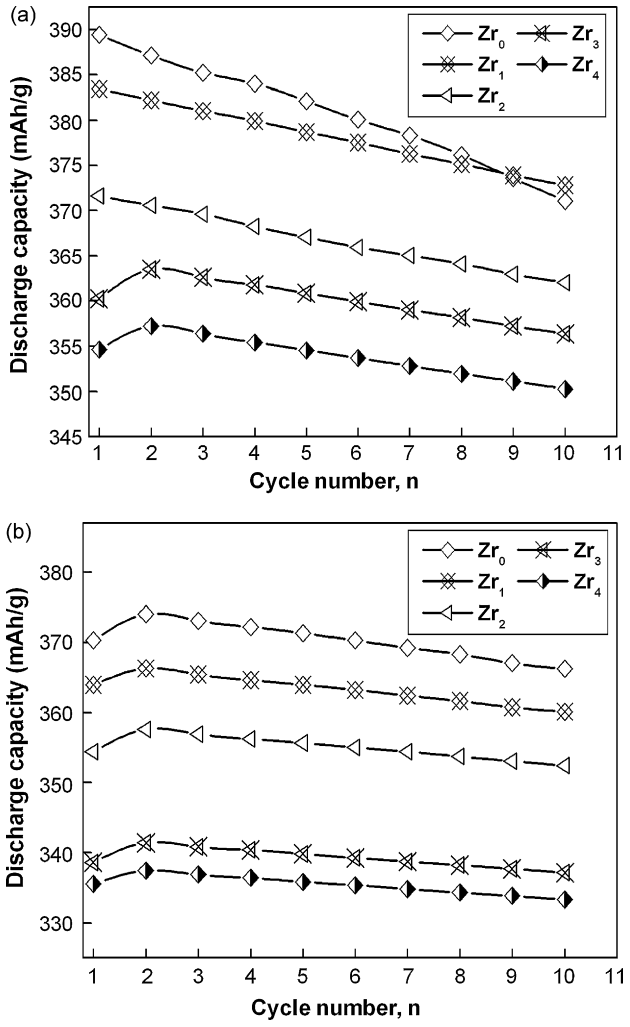


**Fig. 5.** Activation capability of the as-cast and quenched (20 m/s) alloys: (a) as-cast, (b) as-quenched.

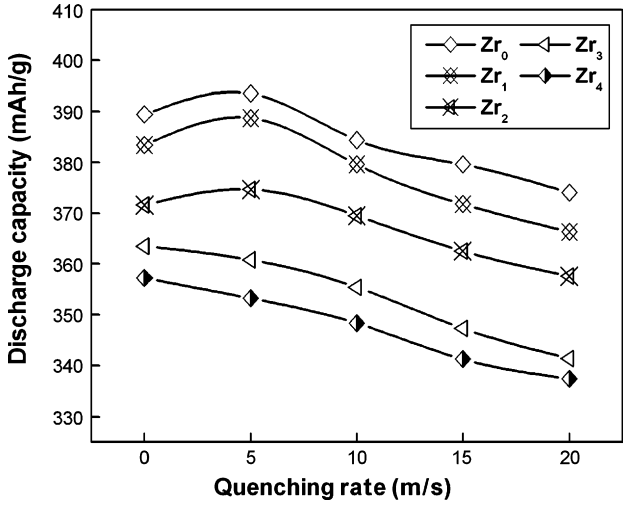


**Fig. 6.** Evolution of the discharge capacities of the alloys with the quenching rate.

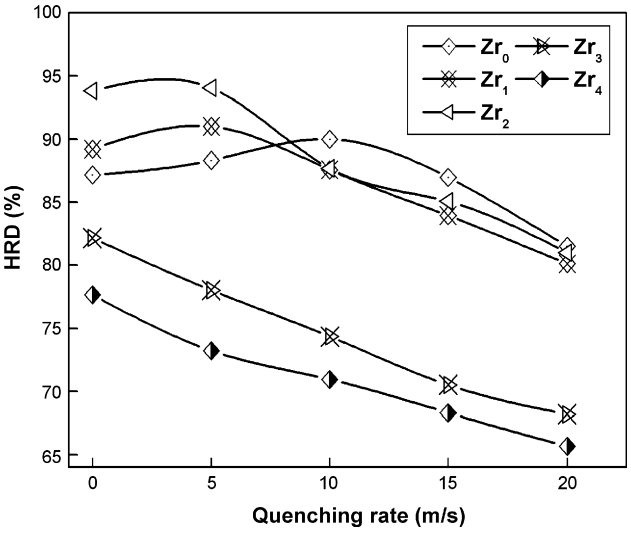


**Fig. 7.** Evolution of the high rate discharge capabilities (HRDs) of the alloys with the quenching rate.

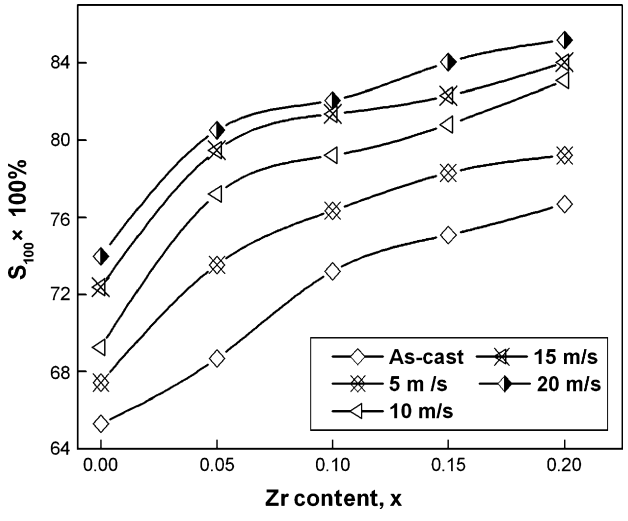


**Fig. 8.** Evolution of the capacity retaining rate ($S_{100}$) of the as-cast and quenched alloys with Zr content.

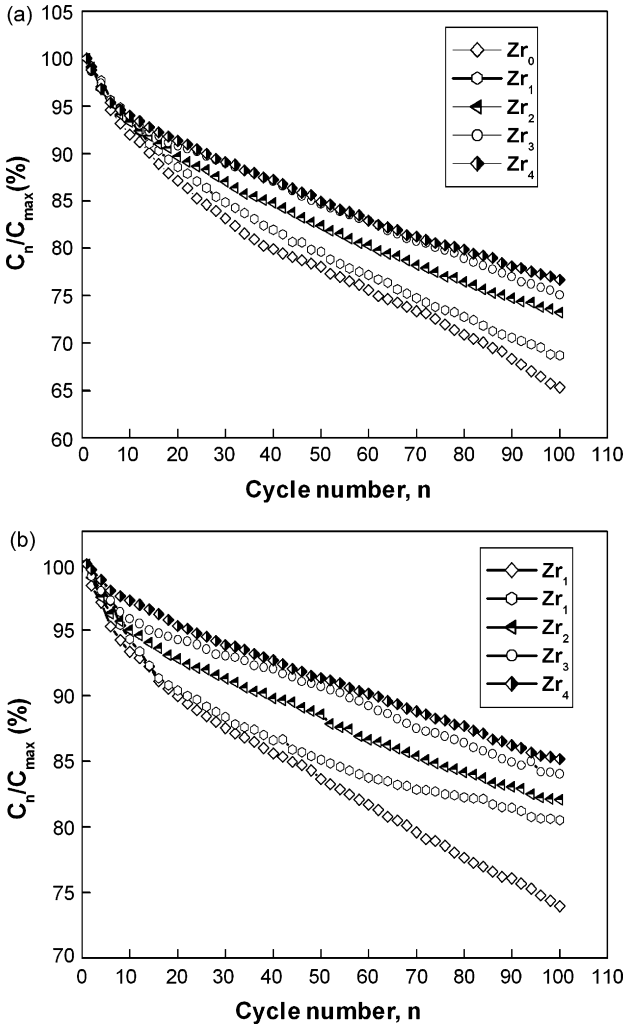


**Fig. 9.** Evolution of the capacity retaining rates of the alloys with the cycle number: (a) as-cast, (b) as-quenched (20 m/s).

be derived in Fig. 8 that for a fixed Zr content the capacity retaining rate ($S_{100}$) of the alloys rises with the increase of the quenching rate, meaning that the rapid quenching clearly improves the cycle stability of the alloys. When quenching rate increases from 0 (As-cast was defined as quenching rate of 0 m/s) to 20 m/s, the capacity retaining rate ($S_{100}$) increases from 65.32% to 73.97% for $Zr_0$ alloy, and from 76.69% to 85.18% for $Zr_4$ alloy. In order to clearly see the process of the capacity degradation of the alloy electrode, the evolution of the capacity retaining rate of the as-cast and quenched (20 m/s) alloys with the cycle number was shown in Fig. 9. A rough tendency can be seen in the Fig. 9 that the substitution of Zr for La causes an obvious decrease of the decay rates of the discharge capacities of the as-cast and quenched alloys, suggesting that the substitution of Zr for La enhances the cycle stability of the alloy.

## 4. Discussion

Based on the systematic analysis of the structures of the as-cast and quenched alloys, some explanations can be provided as reasons for the changes of the electrochemical performances caused by Zr substitution and rapid quenching.

Generally, the activation capability of the hydrogen storage alloy is directly relevant to the change of the internal energy of the hydride system before and after absorbing hydrogen. The larger the additive internal energy, involving the surface energy which

originates from oxidation film formed on the surface of the electrode alloy and the strain energy which is produced by hydrogen atom entering the interstitial sites of the tetrahedron or octahedron of the alloy lattice, the poorer the activation performance of the alloy [14]. Two explanations may be offered as the reason why the substitution of Zr for La impairs the activation performances of the as-cast and quenched alloys. Firstly, the substitution of Zr for La reduces the lattice parameters and cell volumes of the alloys, increasing the ratios of expansion/contraction of the alloys in the process of the hydrogen absorption/desorption, which means increasing the strain energy. Secondly, the substitution of Zr for La leads to the small amount of amorphous phase formed, decreasing the electrocatalytic activity of the alloy electrodes. The influence of rapid quenching on the activation performance of the alloy is complicated. The grain refinement produced by rapid quenching is favorable for the activation capability of the alloy, but the lattice stress caused by rapid quenching is unfavorable for it. Whether rapid quenching will improve or impair the activation capability of the alloy depend on which of above mentioned two factors is predominant. The influence of the rapid quenching on the activation performance is closely relevant to the compositions of the alloy. Therefore, it is understandable that rapid quenching slightly impairs the activation capability of the $Zr_0$, $Zr_1$ and $Zr_2$ alloys, but its influence on the activation capability of $Zr_3$ and $Zr_4$ alloys is negligible.

The discharge capacity of the alloy depends on multiple factors, involving its crystal structure, phase composition and structure, grain size, composition uniformity and surface state, etc. A decrease of a cell volume caused by the substitution of Zr for La is harmful to enhancing the discharge capacity of the alloy. Therefore, it is understandable that the substitution of Zr for La leads to a decrease of the discharge capacities of the as-cast and quenched alloys. In fact, the discharge capacities of the alloys ($x \leq 0.10$) have the maximum values with the variety of quenching rate, whereas those of the alloys ($x > 0.10$) monotonously decrease with increasing quenching rate (Fig. 6), which is relevant to the change of the phase abundances and structure of the alloys caused by the rapid quenching. It can be derived by data in Table 1 that the rapid quenching caused an increase of the $LaNi_5$ phase and a decrease of the (La, Mg)$Ni_3$ phase, which are disadvantageous to the discharge capacity of the alloy due to a fact that the discharge capacity of the $LaNi_5$ phase is less than that of the (La, Mg)$Ni_3$ phase [15,16]. However, it is noteworthy that the $LaNi_5$ phase works not only as a hydrogen reservoir but also as a catalyst to activate the (La, Mg)$Ni_3$ phase to absorb/desorb reversibly hydrogen in the alkaline electrolyte [17]. It is the above mentioned contrary effects that result in an optimum quenching rate for the discharge capacities of the alloys. When Zr content $x > 0.10$, the discharge capacity of the alloy monotonously declines with increasing quenching rate. It was attributed to two factors, i.e. the formation of an amorphous phase and the increase of the $LaNi_5$ phase caused by rapid quenching, which are disadvantageous for the discharge capacity of the alloy. The capacity of the amorphous phase is half as large as that of the crystalline alloy [18]. Therefore, it is self-evident that the discharge capacity of the alloy monotonously declines with increasing quenching rate.

The HRD of the alloy is a dynamical problem of hydrogen absorbing/desorbing of the alloy electrode, which is influenced mainly by the electrochemical reaction kinetics on the alloy powder surface and the diffusion rate of hydrogen in the bulk of the alloy [19]. When Zr content $x \leq 0.1$, the HRDs of the alloys obtain the maximum value with the variety of the quenching rate (Fig. 7). The grain refinement produced by the rapid quenching enhances the diffusion capability of hydrogen in the alloy [20], but the lattice distortion and the internal stress caused by the rapid quenching lower the diffusion capability of hydrogen [21]. It seems to be self-evident that the above contrary effects consequentially result in an optimum quenching rate for the HRDs of the alloys. When Zr content $x > 0.10$, the HRDs of the alloys monotonously fall with the variety of the quenching rate, for which the formation of an amorphous phase is probably responsible.

The cycle stability of the electrode alloy is a decisive factor of the life of the Ni–MH battery. The main cause leading to battery efficacy loss is due to the negative electrode rather than to the positive electrode. The electrode failure is characterized by the decay of the discharge capacity and the drop of the discharge voltage. The literatures [22] revealed that the fundamental reasons for the capacity decay of the electrode alloy are the pulverization and oxidation of the alloy during charging–discharging cycle. The lattice stress and the expansion of the cell volume, which are inevitable when hydrogen atoms enter into the interstitial sites of the lattice, are the real driving force that leads to the pulverization of the alloy. The decrease of the cell volume caused by the substitution of Zr for La increases the ratios of expansion/contraction of the alloys in process of the hydrogen absorption/desorption, which means impairing the anti-pulverization capability of the alloy. However, the substitution of Zr for La significantly improves the cycle stability of the alloy electrode (Fig. 8), for which the increase of the $LaNi_5$ phase caused by Zr substitution is responsible. The positive impact of the rapid quenching on the cycle stability of the alloy is primarily ascribed to the significant refinement of the grains caused by rapid quenching. The anti-pulverization capability of the alloy basically depends on its grain size. Therefore, it is understandable the cycle stability of the alloy increases with increasing quenching rate.

## 5. Conclusions

The structures and electrochemical performances of the as-cast and quenched $La_{0.75-x}Zr_xMg_{0.25}Ni_{3.2}Co_{0.2}Al_{0.1}$ ($x = 0$, 0.05, 0.1, 0.15, 0.2) electrode alloys were investigated, and the conclusions obtained are summarized as following:

1. The substitution of Zr for La did not change the phase compositions of the $La_{0.75-x}Zr_xMg_{0.25}Ni_{3.2}Co_{0.2}Al_{0.1}$ ($x = 0$, 0.05, 0.1, 0.15, 0.2) alloys, but it increased the amount of the $LaNi_5$ phase in the alloys, and obviously reduced the lattice constants and cell volumes of the alloys.
2. For a fixed quenching rate, the discharge capacities of the alloys decreased with increasing Zr content. The substitution of Zr for La slightly impaired the activation performances of the as-cast and quenched alloys, but it enhanced cycle stability of the as-cast and quenched alloys.
3. Rapid quenching exerted an obviously influence on the electrochemical performances of the alloys. Summarily, the discharge capacities and the HRDs of the alloys ($x \leq 0.10$) had the maximum values at a special quenching rate, and it is changeable with the variety of Zr content. Rapid quenching significantly improved the cycle stability of the alloys, which was attributed to the refinement of the grains of the alloys produced by the rapid quenching.

## Acknowledgements

This work is supported by Hi-Tech Research and Development Program of China (2006AA05Z132), National Natural Science Foundations of China (50871050 and 50701011), Natural Science Foundation of Inner Mongolia, China (200711020703) and High Education Science Research Project of Inner Mongolia, China (NJzy08071).

## References

[1] J.J.G. Willems, K.H.J. Buschow, J. Less-Common Met. 129 (1987) 13–30.
[2] S.R. Ovshinsky, M.A. Fetcenko, J. Ross, Science 260 (1993) 176–181.

[3] M. Tsukahara, T. Kamiya, K. Takahashi, A. Kawabata, S. Sakurai, J. Shi, H.T. Takeshita, N. Kuriyama, T. Sakai, J. Electrochem. Soc. 147 (2000) 2941–2944.
[4] D.L. Sun, H. Enoki, F. Gingl, E. Akiba, J. Alloys Compd. 285 (1999) 279–283.
[5] Q.D. Wang, C.P. Chen, Y.Q. Lei, J. Alloys Compd. 253–254 (1997) 629–634.
[6] I. Uehara, T. Sakai, H. Ishikawa, J. Alloys Compd. 253–254 (1997) 635–641.
[7] T. Kohno, H. Yoshida, F. Kawashima, T. Inaba, I. Sakai, M. Yamamoto, M. Kanda, J. Alloys Compd. 311 (2000) L5–L7.
[8] Y.F. Liu, H.G. Pan, M.X. Gao, Y.Q. Lei, Q.D. Wang, J. Alloys Compd. 403 (2005) 296–304.
[9] H.G. Pan, Y.F. Liu, M.X. Gao, Y.F. Zhu, Y.Q. Lei, Q.D. Wang, J. Alloys Compd. 351 (2003) 228–234.
[10] H.G. Pan, Y.J. Yue, M.X. Gao, X.F. Wu, N. Chen, Y.Q. Lei, Q.D. Wang, J. Alloys Compd. 397 (2005) 269–275.
[11] B. Liao, Y.Q. Lei, L.X. Chen, G.L. Lu, H.G. Pan, Q.D. Wang, J. Alloys Compd. 376 (2004) 186–195.
[12] Y.H. Zhang, X.P. Dong, G.Q. Wang, S.H. Guo, J.Y. Ren, X.L. Wang, Int. J. Hydrogen Energy 32 (2007) 594–599.
[13] Y.H. Zhang, B.W. Li, H.P. Ren, Y. Cai, X.P. Dong, X.L. Wang, J. Alloys Compd. 458 (2008) 340–345.
[14] M.S. Wu, H.R. Wu, Y.Y. Wang, C.C. Wan, J. Alloys Compd. 302 (2000) 248–257.
[15] H. Oesterreicher, J. Clinton, H. Bittner, Mater. Res. Bull. 11 (1976) 1241–1247.
[16] T. Takeshita, W.E. Wallace, R.S. Craig, Inorg. Chem. 13 (1974) 2282–2283.
[17] H.G. Pan, Y.F. Liu, M.X. Gao, Y.Q. Lei, Q.D. Wang, J. Electrochem. Soc. 150 (5) (2003) A565–A570.
[18] Y. Li, Y.T. Cheng, J. Alloys Compd. 223 (1995) 6–12.
[19] C. Iwakura, M. Matsuoka, K. Asai, T. Kohno, J. Power Sources 38 (1992) 335–343.
[20] P. Li, X.L. Wang, Y.H. Zhang, R. Li, J.M. Wu, X.H. Qu, J. Alloys Compd. 353 (2003) 278–2882.
[21] Y.H. Zhang, G.Q. Wang, X.P. Dong, S.H. Guo, J.Y. Ren, X.L. Wang, J. Funct. Mater. (Chinese) 37 (2) (2006) 250–254.
[22] D. Chartouni, F. Meli, A. Züttel, K. Gross, L. Schlapbach, J. Alloys Compd. 241 (1996) 160–166.